JOURNAL OF MATERIALS SCIENCE 27 (1992) 6391–6400

Transverse dimensions of wood pulp fibres by confocal laser scanning microscopy and image analysis

H. F. JANG, A. G. ROBERTSON, R. S. SETH
Pulp and Paper Research Institute of Canada, 3800 Wesbrook Mall, Vancouver, British Columbia, Canada V6S 2L9

Cross-sectional images of wood-pulp fibres were generated using optical sectioning by a confocal laser scanning microscope. The technique has a distinct advantage over mechanical sectioning with a microtome, as it simplifies specimen preparation. Cross-sectional images were obtained for unbleached softwood kraft pulp fibres using epifluorescence mode. The accuracy of cross-sectional images was verified by imaging fluorescent microspheres. An image analysis procedure, in which the boundaries of fibre cross-sections were defined with a maximum-gradient edge-finding technique, was developed for measuring fibre cross-sectional area and wall thickness rapidly and accurately. The measurements were insensitive to the confocal microscope's asymmetric resolution, signal deterioration through the specimen thickness, overall image quality and operator bias.

1. Introduction

Coarseness, defined as mass per unit fibre length, is an important pulp property [1]. Although coarseness is a distributed parameter [2], it is difficult to measure rapidly as a distribution. Procedures for finding a numerical average coarseness for pulp fibres in a sheet were established by Clark [3, 4] and later by Ranger [5]. Their method is based on the statistical theory of fibre networks by Corte and Kallmes [6], in which coarseness is related to the number of fibres intersecting a reference line of known length in a random network of known grammage. This method was extended by Jordan *et al.* [7] using image analysis to measure sheet voids. Recently, an optical instrument, the Kajaani fibre length analyser (Kajaani Electronics Ltd, Finland), was developed for rapidly determining the fibre-length distribution. If the total mass of pulp fibres measured by the instrument is known, it will calculate a population-average fibre coarseness. However, there is no comparable rapid method that can provide fibre coarseness as a distribution.

Fibre cross-sectional area and coarseness are related by the density of fibre-wall material. In addition, given the area and centreline perimeter of a fibre cross-section, the mean fibre-wall thickness also can be calculated. Measurements of fibre cross-sectional shape and dimensions recently were made by Kibblewhite and Bailey [2]. They prepared fibre cross-sections by embedding and microtome sectioning, and used image analysis to determine frequency distributions of fibre width, cross-sectional area and wall thickness for a range of softwood kraft pulps. However, specimen preparation by their method is slow, in part because fibres have to be manually aligned perpendicular to the plane of sectioning prior to embedding. Fibres can also be distorted during microtome sectioning.

A new type of light microscope, the confocal laser scanning microscope (CLSM), is becoming increasingly important for the study of three-dimensional morphology in biological systems [8]. The distinct advantage of this new microscope is its ability to generate rapidly nondestructive optical sections in thick translucent specimens such as wood fibres [9].

In this study, a CLSM was used to generate fibre cross-sectional images, from which various transverse dimensions of a fibre were calculated by image analysis (IBAS, Kontron Elektronik GmbH, Germany). Although the CLSM has been used to observe fibre surface structure [10], to our knowledge there is no published work dealing with its use for the quantitative study of fibre properties.

In this paper, a brief introduction is given to the CLSM. The instrument is described, and procedures for preparing fibre sample slides for epifluorescence mode, as well as for generating cross-sectional images are given. The results are presented and discussed.

2. Confocal laser scanning microscope (CLSM)

A CLSM differs from a conventional optical microscope in that it illuminates and images the sample one point at a time. The image is built up, pixel by pixel, by scanning either a laser beam or the sample. Resolution is determined by the diffraction-limited laser spot size. The CLSM has better lateral resolution than the conventional optical microscope [11]. Digital image processing can be used to improve the image signal-to-noise (S/N) ratio and contrast.

0022–2461

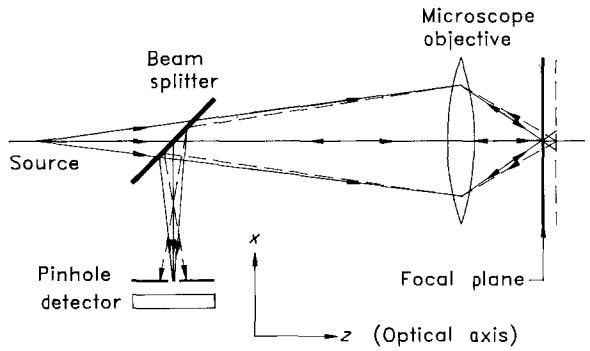

Figure 1 Depth discrimination in the confocal scanning microscope. Epi-illumination makes the single lens serve as both the condenser and objective. The pinhole prevents light originating from anywhere but the plane of focus from reaching the detector. In epifluorescence mode, a blocking filter is used, such that only fluorescent light emitted by the sample is detected. However, in reflected light mode, no filter is used, and both light reflected from sample interfaces and fluorescent light emitted by the sample are detected.

The term "confocal" indicates that both condenser and objective lenses are focused on the same point in the object. In epi-illuminating mode, a single objective lens serve as both condenser and objective for the epifluorescent and reflected light (Fig. 1). A pinhole in front of the photodetector obstructs most of the scattered, reflected or fluorescent light from out-of-focus planes. A thin layer within a thick translucent object can be imaged clearly; the pinhole ensures that image information is obtained from only one particular plane in the specimen. The pinhole also reduces image blurring due to light scattering, thus increasing the effective resolution [12].

Optical sectioning makes it possible to reconstruct, by software, two different types of image from a three-dimensional image data block, which is comprised of a stack of two-dimensional images acquired over the depth of a thick translucent object. The image slices in such a three-dimensional block can be added to give a two-dimensional image that is in focus throughout the entire depth of the original block – an image which cannot easily be generated with a conventional optical microscope. Alternatively, given visualization software, it can be displayed, rotated and manipulated as a three-dimensional structure [13].

3. Experimental procedure

A Bio-Rad MRC-500 CLSM with improved MRC-600 optics, attached to a Zeiss Axiophot microscope, was used for the present study. The light source was a 25 mW argon ion laser with excitation wavelengths at 488 and 514 nm. In most cases, a neutral density filter was used to reduce the intensity of the laser. The automatic gain control for the photomultiplier was disabled to minimize the non-linearity in the response which was a problem in quantitative measurements. All observations were made with a $\times 100$ oil immersion Plan-Apochromatic objective with a numerical aperture of 1.3. The resolution of the system was asymmetric; the lateral resolution was about 0.25 μm, while the axial resolution was poorer.

To generate a cross-sectional image, a fibre was first oriented perpendicular to the horizontal scanning direction. In a CLSM, as in a conventional light microscope, the focal plane is fixed relative to the optics; in order to scan the image plane through the depth of an object, the object itself must be moved along the optical axis. The cross-sectional (x–z) images presented here were constructed from a series of horizontal line scans acquired while stepping the sample stage vertically in the z-direction. Typically, the smallest step size available, 0.16 μm, was used, and up to 50 scans per step were averaged to increase the S/N ratio. Generating a single cross-sectional image by scanning 20.48 μm through the depth of a fibre (128 levels at 0.16 μm stepping), at 50 scans averaged per level, took 30 s.

The pulp used for these experiments was western Canadian spruce unbleached kraft. Because unbleached fibres are only weakly auto-fluorescent, to generate a good image quickly in fluorescence mode it was necessary to dye fibres with fluorochrome dye. After dyeing, fibres were washed thoroughly to remove excess dye. Dyed fibres were dried on microscope slides, and then were mounted in Permount medium and covered with cover slips. Permount was used because its refractive index n was close to that of the fibres, microscope slides and cover slips ($n \approx 1.5$). A mounting medium with a different refractive index can create serious imaging problems (see Appendix).

Fluorescence images were obtained with two sets of excitation filters: blue (488 nm, "BHS" set) and green (514 nm, "GHS" set) (Bio-Rad Microscience, Canada). Reasonable fluorescence images were obtained for all fibres, using different dyes, dyeing conditions and filters. However, the strongest fluorescence signals were obtained with fibres weakly dyed in Acridine Orange, with the BHS blue excitation filter set. This combination was used in our study. Lightly dyed fibres gave better images, because signals deteriorated rapidly through the thickness of a strongly dyed fibre. Most results presented here were for fibres dyed at room temperature in a very dilute solution (0.01 g dye diluted in 1 l water), with dyeing times of between 2 and 10 min.

Fluorescent calibration microspheres (Polysciences, PA, USA) were diluted and dried on microscope slides, mounted in Norland (Norland Products, NJ, USA) adhesive ($n = 1.524$) and covered with cover slips. To cure the adhesive, slides were irradiated for about 5 min with ultraviolet light.

4. Results and discussion

Fig. 2a–f show typical cross-sectional images of fibres using vertical optical sectioning in epifluorescence mode CLSM. These images reveal the shapes of air-dried fibres. Fibres with thin walls were almost totally collapsed, as shown in Fig. 2a and b. As the thickness of fibre walls increased in subsequent images in Fig. 2, fibres were less collapsed.

Some images suggested that the dried fibre surfaces were not smooth, but the details were unclear. Reflected light mode is more sensitive than fluorescence

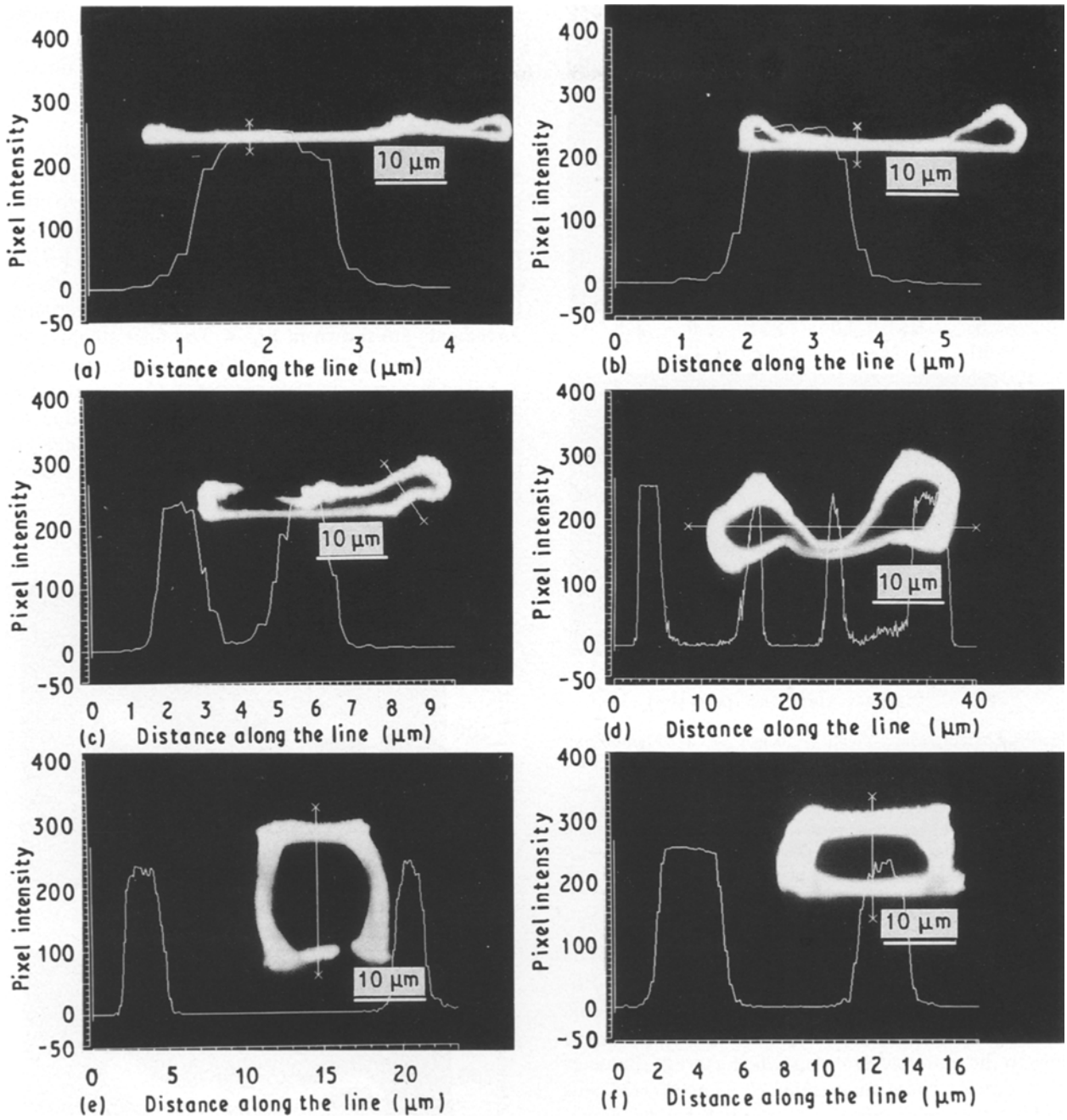

Figure 2 Epifluorescence cross-sectional images of lightly fluorochrome-dyed fibres. Fluorescent signals were weaker and noisier in the lower parts of thick-walled fibres due to self-shadowing.

mode to fibre surface structure [14], and has been used to observe surface structure during the drying of pressed wet webs made of hardwood bleached kraft pulp [10].

In general, image quality deteriorated as the objective was focused deeper into the fibres. Fluorescent signals were weaker and noisier, and the grey level profile transitions at the fibre edges, which correspond to section lines marked x–x in the figures, were less sharp (e.g. compare the top and bottom profiles in Fig. 2e and f). This was due to two independent effects: (i) cumulative photobleaching when line-scanned from the top to the bottom of fibre; and (ii) the fibre itself attenuating both the excitation and the resulting fluorescent signal intensity, by scattering and absorption. This second factor is known as "self-shadowing" in epifluorescent mode [15]. It was more pronounced for fibres which were heavily dyed. High laser intensity was not desirable, because it rapidly photo-bleached the fluorochrome dye. What was needed was to dye fibres weakly, using a dye with high fluorescence quantum efficiency and high resistance to photo-bleaching. In the present study, the signal from the bottom of a 20 μm deep vertical wall was still of reasonable quality (Fig. 2e and f). While images were sharper in horizontal parts than in vertical, asymmetric resolution is best illustrated with the images of microspheres presented next.

To establish the validity of the CLSM cross-sectional images and the accuracy of the measurements, fluorescent calibration microspheres were used (Fig. 3). To illustrate the lateral resolution of CLSM, Fig. 3a shows the largest horizontal (x–y) cross-sectional image of a microsphere that has a diameter

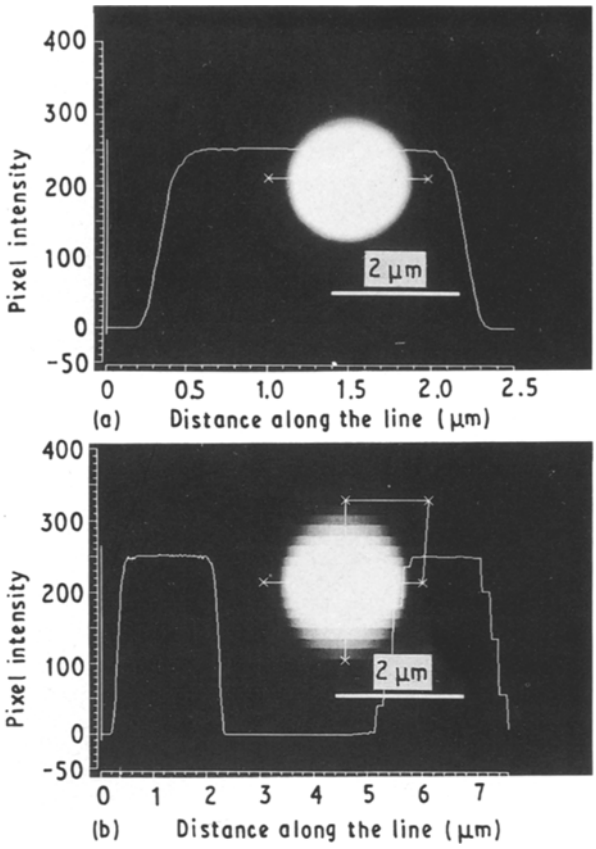

Figure 3 Epifluorescence confocal images of a "Fluoresbrite" microsphere: an x–y section image is shown in (a) and an x–z orthogonal section image in (b). The grey-level profiles for the lines shown x–x are plotted. These images and profiles show that lateral resolution was better than axial. However, the full-width-half-maximum (FWHM) sphere diameters obtained from the x- and z-direction profiles of (b) were similar.

comparable to typical fibre-wall thicknesses. The cross-section was circular, as expected. The full-width-half-maximum (FWHM) of the grey level profile across the middle of this image was 1.9 μm. This was close to the manufacturer's specified average diameter of 2.0 μm for these microspheres. The FWHM was used because, in the ideal case, the half-height intensity of the fluorescence grey-level profile for a scanning line which is perpendicular to an object's surface corresponds to the centre of the laser spot being located at that surface.

To establish the validity of vertical (x–z) cross-sectional images, Fig. 3b shows a vertically-scanned image of the same microsphere taken through the centre of the sphere. The image in Fig. 3a was circular; however, the x–z cross-sectional image in Fig. 3b was elongated in the z-direction. The profiles for both the horizontal (x-axis) and vertical (z-axis) section lines of the image are plotted. The transition in grey-level at the microsphere edge in the x-direction was about 0.25 μm wide, whereas the intensity transition in the z-direction was about 0.7 μm wide. This clearly illustrates that axial resolution was lower than lateral. Despite this, the FWHM of the horizontal and vertical profiles in Fig. 3b were the same: 1.9 μm. That is, although much lower resolution was observed in the z-direction, its FWHM value was similar to that obtained in the x-direction of this cross-sectional image. FWHM values can be regarded as the diameters of the microspheres; however, a different and better method was used to measure the dimensions of microspheres and fibres, as will be discussed below in the image analysis section.

With an objective lens of 1.3 numerical aperture and 488 nm excitation, the theoretical resolution in the z-direction is about 0.5 μm [16]. According to the Nyquist sampling theorem, a minimum of 2.3 pixels per optically resolvable element are needed [17]. This implies that stepping should be finer than about 0.2 μm. Images obtained from three different stepping increments are shown in Fig. 4. The finer stepping in Fig. 4c improved the image. For example, cross-sectional edges were relatively smooth in Fig. 4c, but were discontinuous or stepped in Fig. 4a and b due to undersampling. Apart from Fig. 4a and b, all images in this work were obtained with the smallest available stage stepping increment of 0.16 μm.

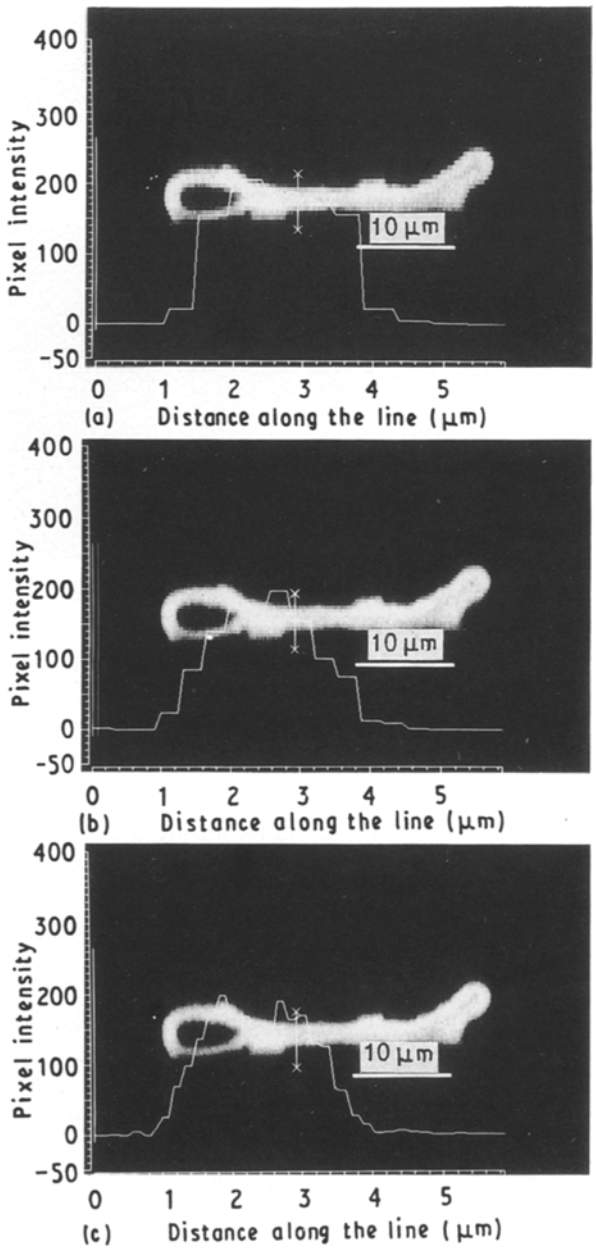

Figure 4 Fibre cross-sections with three different stage stepping increments on the z-axis: (a) 0.48 μm, (b) 0.32 μm and (c) 0.16 μm.

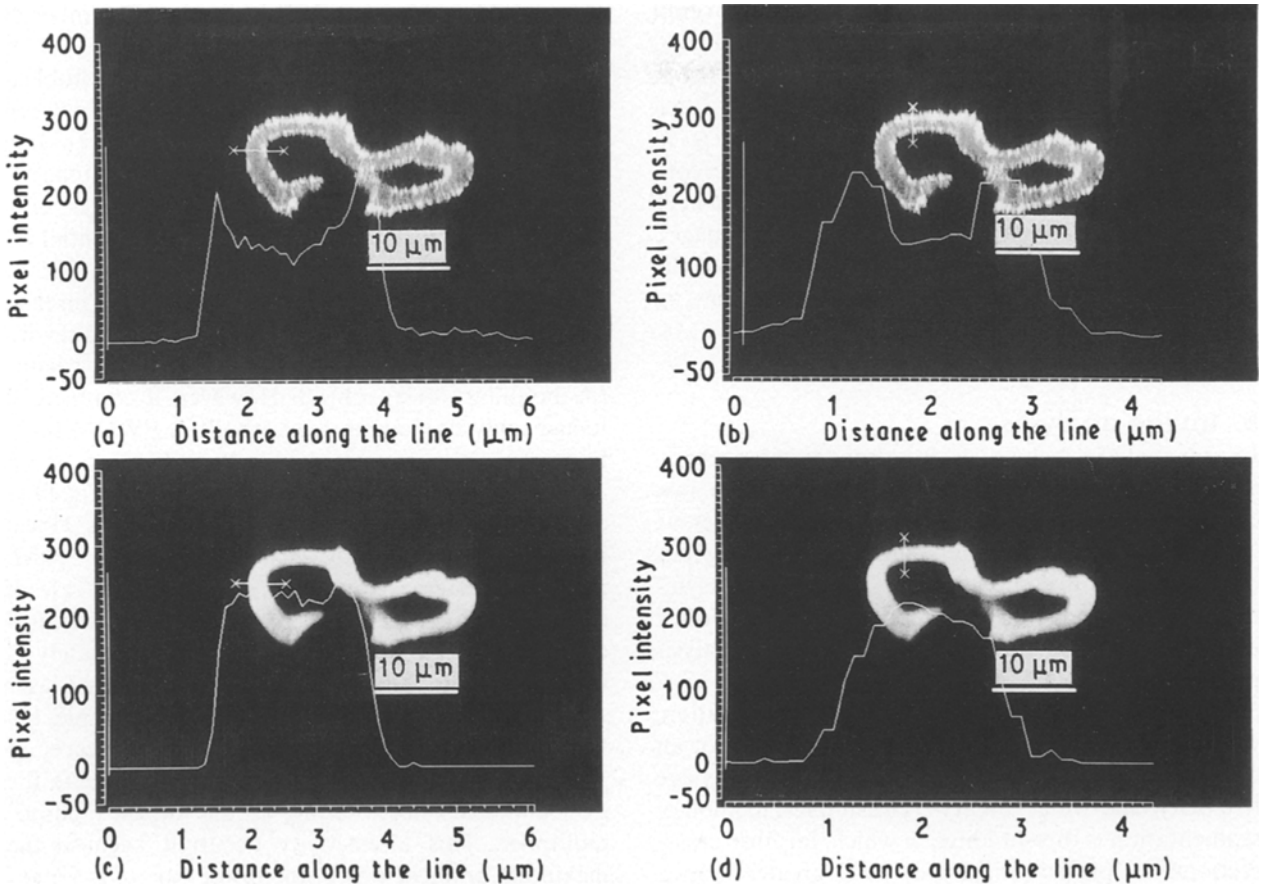

Figure 5 Images of the same cross-section of a fluorochrome-dyed fibre. The same area of the fibre was used for both (a, b) reflected light and (c, d) epifluorescence images. The grey-level profiles in (a) and (c) were horizontal, while those in (b) and (d) were vertical.

Unlike fluorescence images, reflected light confocal images revealed only the outlines of fibre walls [14]. This was because reflection occurs only at the interface of two media with different refractive indices. If there is no multiple reflection between fibre walls, the central peaks of the reflected intensities from the interfaces between fibres and mounting medium can be accurately defined as the location of the fibre surface boundaries. However, because reflected light images lose information on tilted surfaces such as vertical fibre walls [14], it was not practical to use this imaging mode to obtain the dimensions of fibre cross-sections.

In this study, the ability of the reflection mode to outline the fibre surface was used to confirm the accuracy of fluorescence images. This was done by comparing fluorescence and reflected light mode images of the same fluorochrome-dyed fibre. The reflected light images in Fig. 5a and b were very similar to the corresponding fluorescence images in Fig. 5c and d. The reflected images were interpreted as the weighted sum of the reflected and fluorescent signals, and were simulated by a simple model (Fig. 6). In this figure, a theoretical axial grey-level profile across a vertical section image of an object with finite thickness and flat reflective surfaces was used to simulate the reflection component in images of fibre walls [14]. For the calculated fluorescence component, the FWHM of the profile was set equal to the true fibre-wall thickness, with the profile transition on each side taken from the theoretical reflection component.

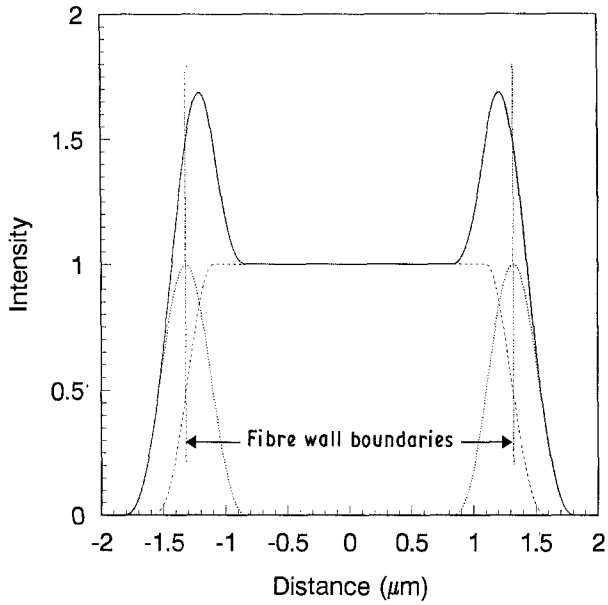

Figure 6 A simple model for interpreting reflected light images of fluorochrome-dyed fibres. The two peaks with maxima located at the fibre-wall boundaries were theoretically derived [16] and had FWHM of 0.45 μm. (· · ·) Reflected light signal component, (---) fluorescence signal component, (——) total signal in reflection mode.

The general shape of the resultant grey-level profile, summed with fluorescence and reflected components having equal weights, as shown in Fig. 6, was very similar to the reflected mode profiles in Fig. 5a and b. According to this model, the true fibre-wall edges were

located slightly outside the two peaks in the overall reflected image signal. Consistent with this result, comparing Fig. 5a and c with b and d, the FWHM of the fluorescence profiles in Fig. 5c and d were located slightly outside the two corresponding peaks in Fig. 5a and b, respectively. That is, these images were consistent with the proposed model, and the fluorescence images were consistent with the reflected light images. The model also suggested that the intensities of the reflected light and fluorescence signal components in Fig. 5a and b were comparable.

5. Image analysis

Image analysis techniques for deriving fibre cross-sectional area and average wall thickness from raw confocal cross-sectional images are discussed below. Making quantitative measurements by image analysis of such images is complicated by the CLSM's asymmetric resolution and self-shadowing, and operator bias in CLSM instrument settings and image analysis procedures.

The first step in analysing an image is segmentation, which involves identifying the true boundaries of an object in an image, while reducing a grey-level image to a black-and-white "binary". The simplest method of segmentation is thresholding, in which, for fibre cross-sections, all pixels with a grey level greater than a selected value are interpreted as fibre wall, and all others as background. The area of a fibre-wall cross-section then is determined by counting the number of segmented wall pixels.

In this study, when self-shadowing and photobleaching produced differences in pixel intensities between upper and lower parts of a fibre image, thresholding segmented inconsistently. The greater the difference in intensities between brighter and darker sides of a cross-sectional image, the greater was the potential for error.

As stated earlier, the FWHM value is rather insensitive to the asymmetric resolution and variable intensities in a CLSM image, and could be used to define the boundary of an object. However, a commercial image analyser may not have a built-in FWHM function.

A better way to identify the boundaries of a fibre cross-section is to use the image analyser's "local maximum gradient" edge-detection function, which picks out image regions with a high spatial rate of change of grey level. The positions at which the gradient has its peak values correspond approximately to the locations at which the centre of the scanned laser spot was located at the fibre surface. In principle, the FWHM and gradient methods are similar; however, in practice, the gradient method was less sensitive to the gain and black level setting of the CLSM's photomultiplier. This insensitivity occurred because the maximum gradient was in the lower part of the grey-level profile for a low-gain image, but shifted to the upper part of the profile as the gain was increased.

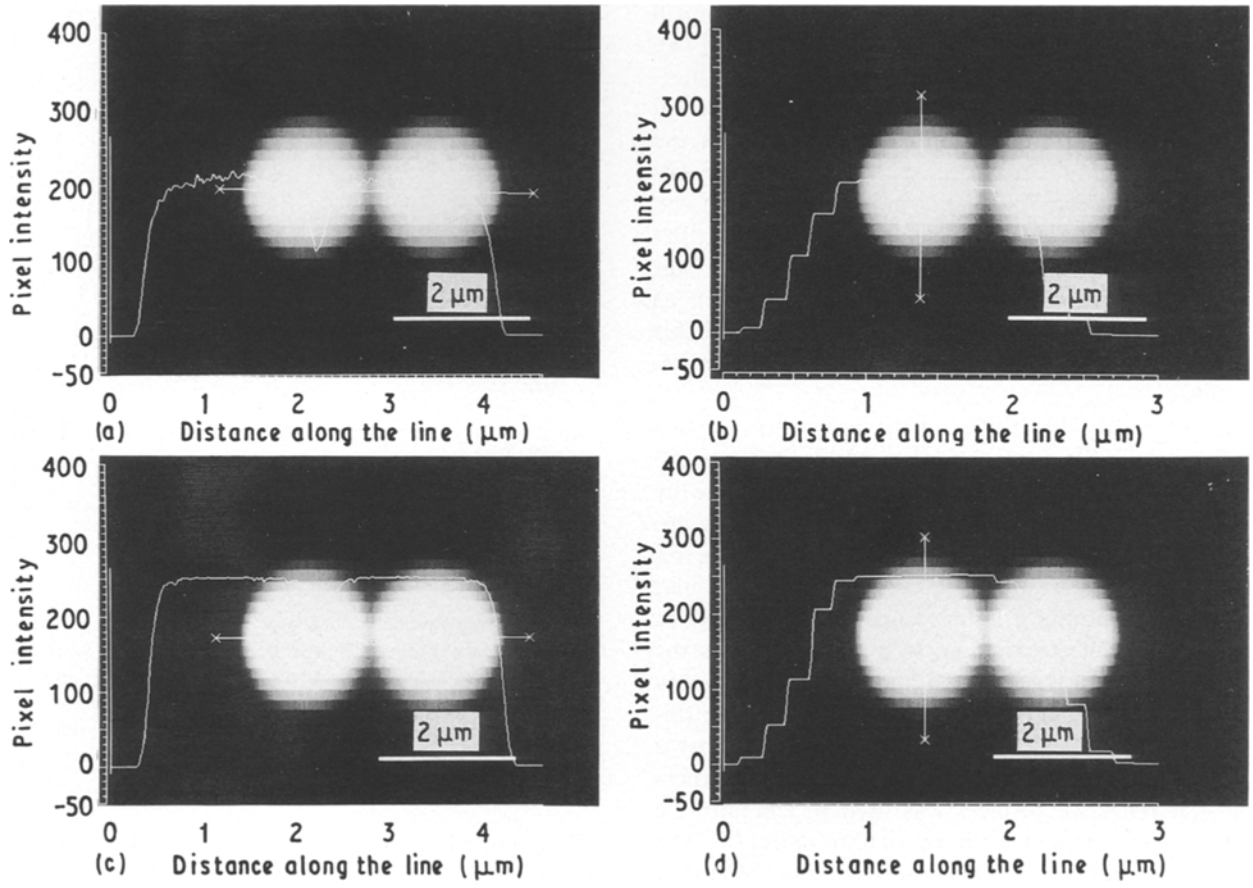

Figure 7 Epifluorescence confocal images of two touching microspheres at two different photomultiplier gain levels. The images in (a) and (b) were acquired at a low photomultiplier gain; (a) shows a horizontal grey-level profile, and (b) a vertical. The images in (c) and (d) were acquired at a higher gain, and have horizontal and vertical profiles, respectively.

TABLE I Image analysis results for microspheres

Figure	Cross-sectional area, A (μm^2) (calculated diameter, $D = 2(A/\pi)^{1/2}$ (μm))	Circumference, C (μm) (calculated diameter, $D = C/\pi$ (μm))
3a	2.76 (1.87)	5.90 (1.88)
b	2.82 (1.89)	5.98 (1.90)
7a	5.35 (1.85)[a]	
c	5.52 (1.88)[a]	

[a] Average diameter for a microsphere in the pair.

This is illustrated by the images of two touching spheres shown in Fig. 7.

In this figure, two sets of fluorescence images were acquired with different photomultiplier gains. From the profiles of these images, the FWHM in the x- and z-directions increased from 3.7 μm (the total diameter for two spheres in Fig. 7a) and 1.7 μm (the diameter of one sphere in Fig. 7b), to 3.8 and 1.9 μm in Fig. 7c and d, respectively, as the gain increased.

Using procedures which will be discussed, the cross-sectional areas, A, of the microsphere pairs were 5.35 and 5.52 μm^2 for Fig. 7a and c, respectively (Table I). The diameter, D, of a single sphere, calculated from A, increased from 1.85 μm to 1.88 μm. These variations with gain were smaller than for the FWHM method.

The gradient edge-finding technique was applied to a series of x–z cross-section images of microspheres ranging in size from 0.66–5.85 μm. The resulting edge-contour images were very close to circular, especially for microspheres with sizes larger than 1 μm. The area, A, and circumference, C, of the microspheres for the x–y cross-section in Fig. 3a were 2.76 μm^2 and 5.90 μm, giving $D = 1.87$ and 1.88 μm, respectively. Similarly, A and C for the x–z cross-section in Fig. 3b were 2.82 μm^2 and 5.98 μm, respectively, and the corresponding D were 1.89 and 1.90 μm. These results for x–y and x–z cross-sections were consistent and agreed with the 1.9 μm obtained with the FWHM method.

The image-processing procedures used to obtain cross-sectional areas and average wall thickness are illustrated in Fig. 8. The objective in this processing sequence was to identify the peak of the local maximum gradient as the boundary of the fibre wall. Fig. 8a shows the original confocal image of a fibre cross-section. Before applying the edge-finding technique, a median (or Gaussian) smoothing filter was used to suppress noise (Fig. 8b). Then, a gradient edge-finding filter was applied (Fig. 8c). The image in Fig. 8c was smoothed to help identify the location of the most probable peak (Fig. 8d), and then was thinned (Fig. 8e). Thresholding was applied to convert the grey-level edge image to binary, so that the majority of the edge was represented by one pixel and boundaries were well connected (Fig. 8f). Steps b–f can be replaced by a Canny function [18]. Another thinning was applied to reduce the boundaries to a single pixel thickness (Fig. 8g). Finally, the region between the outer and inner boundaries was filled (Fig. 8h). The fibre cross-sectional area, determined by counting the number of wall pixels, was 140 μm^2.

The average fibre-wall thickness was determined by dividing the wall cross-section area by its centreline length [2]. For uncollapsed fibres, the length of the centreline was calculated after thinning the wall to a single pixel thickness (Fig. 8h). For collapsed fibres where the two inner fibre walls touched (e.g. Fig. 2a, b), more complex procedures were required to obtain the wall centreline. Fig. 8h shows the fibre-wall centreline superimposed on the segmented fibre cross-section. The length of this centreline was 53.0 μm, giving an average wall thickness of 2.64 μm.

These image analysis procedures were rapid and accurate, and rather independent of operator bias. Table II shows the cross-sectional areas, A, perimeters, P, and average wall thicknesses, T, for images presented in the previous figures. The average fibre wall thicknesses for the fibres in Fig. 2 ranged from 1.0–3.99 μm.

Using a smaller z-axis step size (Fig. 4a–c) improved the details of an image, but did not strongly affect the results: the numerical values for A, P and T from all three images agreed (Table II). However, it still was preferable to have a smaller step size, because an edge-finding technique was used to define object boundaries in an image. Instead of giving a smooth boundary for a fibre (such as is shown in Fig. 8g), images with a large step size (e.g. Fig. 4a) produced a roughly stepped, discontinuous boundary, caused by the abrupt changes of intensity in the z-direction in the raw images.

To check how image quality affected the results, pairs of images were produced simultaneously (Fig. 9). The right-hand images were normal fluorescence images, while the left-hand images were obtained by "splitting off" signals and reflecting them to the second detector channel. Signals reaching this second detector were weaker and noisier. However, for images in this figure, the results in Table II show that although the left images were poorer, measurements on

TABLE II Image analysis results for fibres

Figure	Cross-sectional area, A (μm^2)	Perimeter, P (μm)	Average wall thickness, T (μm)
2a	100	100	1.00
b	96.9	85.0	1.14
c	111	65.3	1.70
d	197	89.7	2.20
e	166	51.3	3.24
f	205	51.4	3.99
4a	107	72.0	1.49
b	110	72.2	1.52
c	104	72.0	1.44
8	140	53.0	2.64
9a(L)	72.8	39.5	1.84
a(R)	77.3	39.0	1.98
b(L)	88.3	41.3	2.14
b(R)	94.5	41.1	2.30

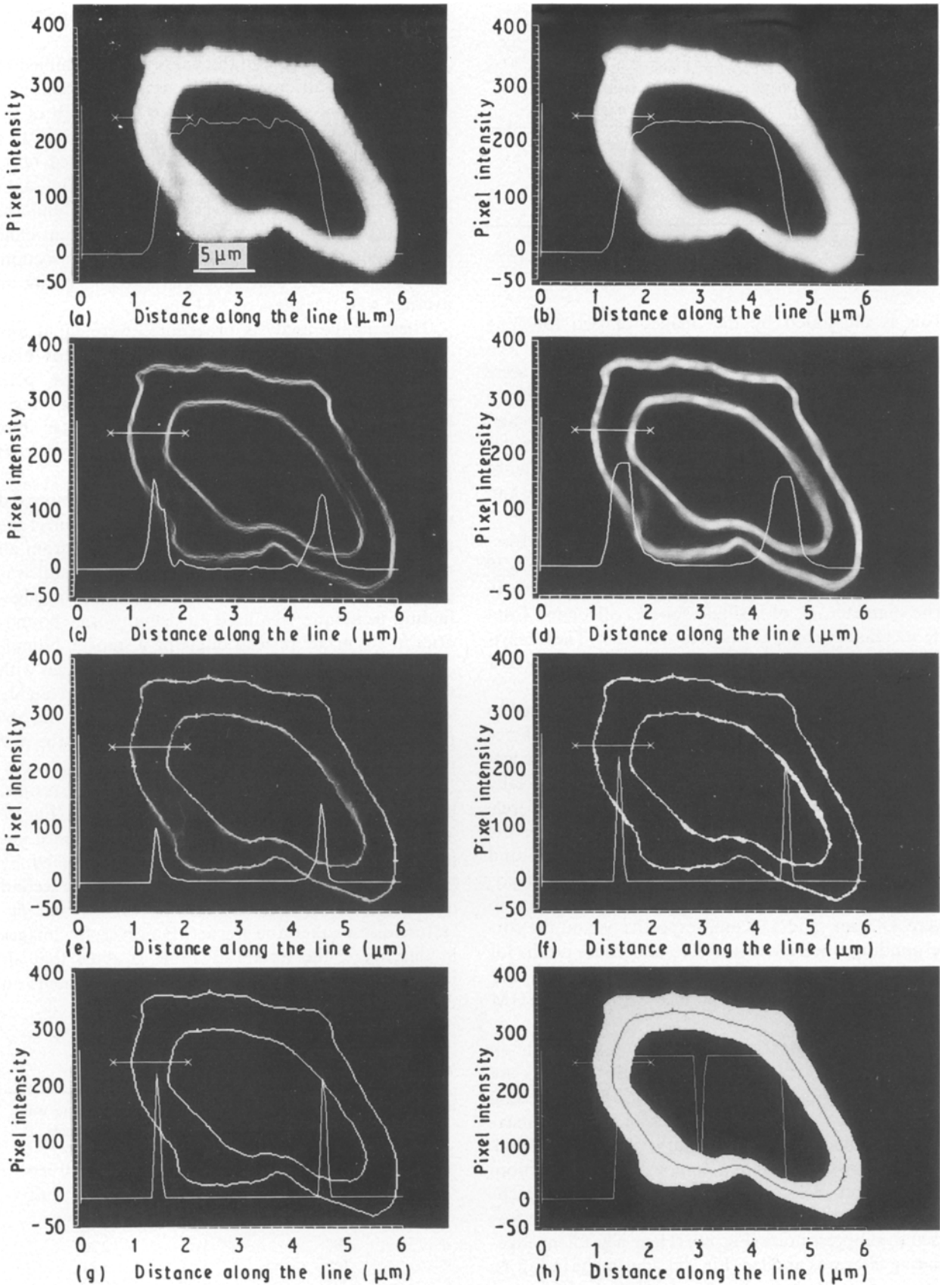

Figure 8 Image analysis procedures to determine fibre cross-sectional area and perimeter: (a) original confocal image, (b) image smoothed by a median (or Gaussian) filter, (c) edges found by using the maximum local gradient, (d) edges smoothed and (e) thinned to such an extent that fibre surface was still well connected, (f) grey-level edges thresholded to binary, (g) another thinning applied to reduce the boundaries to a single pixel thickness, (h) the region between the outer and inner boundaries filled, and a pixel-wide fibre centreline superimposed on to the fibre cross-section.

them agreed within 7% with those obtained from the images on the right. This demonstrates that the procedures used for image analysis were relatively insensitive to noise and resolution.

6. Conclusions

Epifluorescence images of fibre cross-sections for an unbleached softwood kraft pulp and microspheres were obtained by optical sectioning using a CLSM.

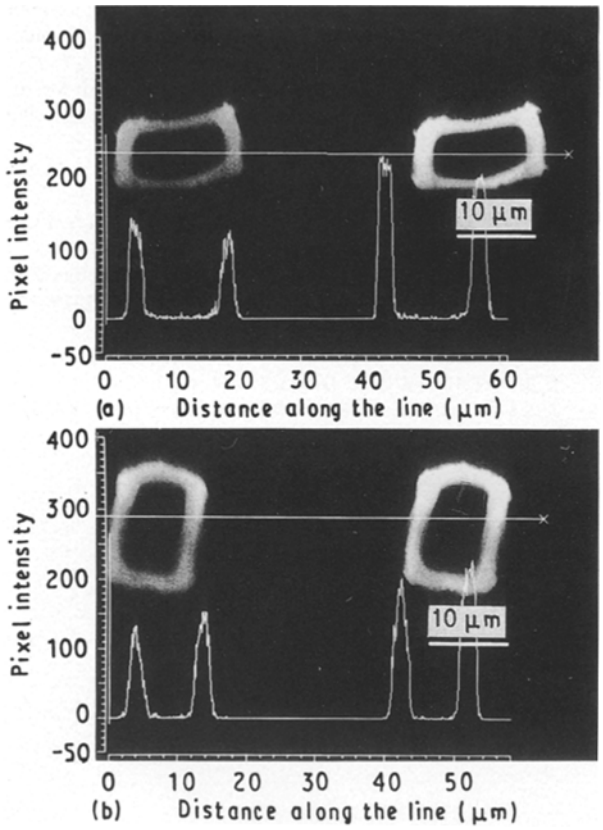

Figure 9 Epifluorescence cross-sectional images of fibres. Images in pairs were taken simultaneously. The signal for the left image in each pair was "split off" from the signal for the right one.

Cross-sectional images of microspheres validated this technique for quantitative measurements.

Weakly fluorochrome-dyed fibres gave more uniform signals than undyed fibres. The best confocal images were obtained from fibres lightly dyed with Acridine Orange, using blue light excitation. Self-shadowing made strong dyeing undesirable, especially for thick-walled fibres. Matching the index of refraction of the mounting media and fibres was essential for obtaining high-quality images. A small z-axis step size gave images with finer details, and facilitated image analysis.

Both maximum gradient edge-finding and FWHM techniques were used to define the boundaries of fibre cross-sections. Both techniques provided consistent results with test microspheres, despite the confocal microscope's asymmetric resolution. The gradient method was preferable because it was less sensitive to the photomultiplier gain level than the FWHM method. Procedures for image analysis were insensitive to signal deterioration through the specimen thickness, overall image quality, and operator bias. CLSM fibre cross-sectional images were processed to yield accurate areas and average wall thicknesses.

Confocal microscopy combined with image analysis offers an accurate and rapid method for determining transverse dimensions along the length of a fibre and in a fibre population. It now is practical to determine distributions of transverse dimensions in fibre populations.

Acknowledgements

We thank George Williams for his guidance in microscopy and specimen preparation, Ben Chan for image analysis, Dr John Carlson, University of British Columbia, for use of the Bio-Rad CLSM, Palitha Dharmawardhana for CLSM technical support, and the Science Council of British Columbia for a post-doctoral fellowship to H. F. Jang.

Appendix. Imaging problems with media of different refractive indices

In Fig. A1, the beam originally is focused in a medium with refractive index $n = 1.5$. If an object with different n (e.g. $n = 1.3$) is inserted into the optical path, light paths are modified according to Snell's law

$$n_1 \sin\Theta_1 = n_2 \sin\Theta_2 \qquad \text{(A1)}$$

where the angle for incident light, Θ_1, is changed to Θ_2, for the refracted light at the interface of two media. In this case, the beam is no longer focused to a single spot; instead, it is dispersed, as shown in the enlarged rectangular box, and the focal plane of the objective is shifted, moving upwards when n_2 is greater than n_1, as in this case. The unfocused beam degrades the resolution of an image. The degradation usually is worse for axial resolution than for lateral, because the beam is more dispersed along the optical axis. For example, if the slab in Fig. A1 were not tilted, the focused beam would be dispersed only along the optical axis (spherical aberration). The shift of the focal plane will produce an image with apparent depth which is different from the actual depth, making axial dimensions incorrect in cross-sectional images.

In this work, in order to obtain the best images, it was important to keep the refractive index constant for all media along the light path. Immersion oil, cover glasses, fibres and microscope slides all had similar refractive indices: $n \approx 1.5$. Permount usually was used as a mounting medium, because its refractive index is approximately 1.5.

CLSM images of fibres suspended in water, acquired with an oil immersion objective, were of low

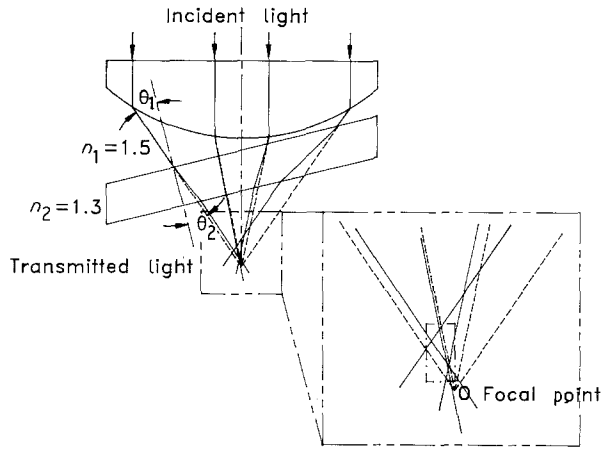

Figure A1 Diagrammatic representation of the effect of inserting a medium with a different refractive index between the objective lens and focal plane. The focal plane is shifted and the focal point is dispersed.

quality, particularly with respect to axial resolution, because of the significantly lower index of refraction of water ($n = 1.3$)

References

1. R. S. SETH, "MRS Symposium Proceedings 197" (Materials Research Society, Pittsburg, PA, 1990) p. 143.
2. R. P. KIBBLEWHITE and D. G. BAILEY, *Appita* **41** (1988) 297.
3. C. T. BRADY, A. BERZINS and J. d'A. CLARK, *Tappi* **39** (1956) 40.
4. J. d'A. CLARK, *Tappi* **45** (1962) 628.
5. A. E. RANGER, *Paper Technol.* **2** (1961) 169.
6. O. KALLMES and H. CORTE, *Tappi* **43** (1960) 737.
7. B. D. JORDAN, N. G. NGUYEN and D. H. PAGE, *Paperi ja Puu* **64** (1982) 691.
8. J. B. PAWLEY (ed.) "Handbook of Biological Confocal Microscopy" (Plenum Press, New York, 1990).
9. H. F. JANG, A. G. ROBERTSON and R. S. SETH, *Tappi J.* **74** (1991) 217.
10. H. NANKO and J. OHSAWA, *J. Pulp Paper Sci.* **16** (1990) J6.
11. T. WILSON and C. SHEPPARD, "Theory and Practice of Scanning Optical Microscope" (Academic Press, London, 1984).
12. S. INOUE in "Handbook of Biological Confocal Microscopy", edited by J. B. Pawley (Plenum Press, New York, 1990) p. 1.
13. A. G. ROBERTSON, H. F. JANG and R. S. SETH, *J. Mater. Sci. Letters* (in press).
14. H. F. JANG, A. G. ROBERTSON and R. S. SETH, to be submitted.
15. P. C. CHENG and R. G. SUMMERS, in "Handbook of Biological Confocal Microscopy", edited by J. B. Pawley (Plenum Press, New York, 1990) p. 179.
16. T. WILSON, *ibid.*, p. 113.
17. R. H. WEBB and C. K. DOREY, *ibid.*, p. 41.
18. J. CANNY, *IEEE Trans. Patt. Anal. Mach. Intell.* **PAMI-8** (1986) 679.

Received 16 July 1991
and accepted 11 March 1992